



Contents lists available at SciVerse ScienceDirect

Spectrochimica Acta Part A: Molecular and Biomolecular Spectroscopy

journal homepage: www.elsevier.com/locate/saa

Complex formation, thermal behavior and stability competition between Cu(II) ion and Cu⁰ nanoparticles with some new azo dyes. Antioxidant and in vitro cytotoxic activity

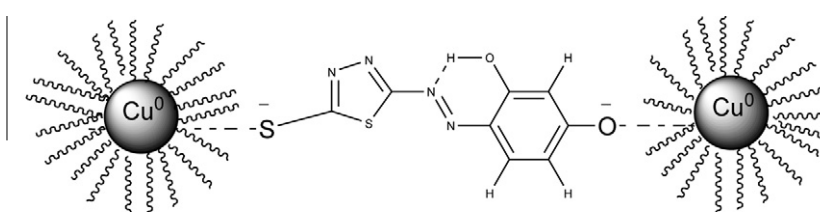
M. Gaber*, Y.S. El-Sayed¹, K.Y. El-Baradie², R.M. Fahmy

Chemistry Department, Faculty of Science, Tanta University, 31527 Tanta, Egypt

HIGHLIGHTS

- ▶ Cu(II) complexes of four triazole and thiadiazole-based azo chromophore were synthesized and characterized.
- ▶ The mode of interaction between the synthesized azo ligands and copper nanoparticles was studied.
- ▶ The antitumor and antioxidant activities of the synthesized azo ligands and their Cu(II) azo complexes have been evaluated.

GRAPHICAL ABSTRACT



The mode of interaction between HL⁴ with the surface of colloidal Cu⁰

ARTICLE INFO

Article history:

Received 25 October 2012
 Received in revised form 25 December 2012
 Accepted 11 January 2013
 Available online 31 January 2013

Keywords:

Azo
 Complexes
 Copper nanoparticles
 Antitumor
 Antioxidant

ABSTRACT

Four triazole and thiadiazole-based azo chromophores namely [(E)-4-((1H-1,2,4-triazol-3-yl)diazonyl)benzene-1,3-diol.(HL¹), (E)-4-((5-(methylthio)-1H-1,2,4-triazol-3-yl)diazonyl)benzene-1,3-diol.(HL²), (E)-4-((1,3,4-thiadiazol-2-yl)diazonyl)benzene-1,3-diol.(HL³) and (E)-4-((5-mercapto-1,3,4-thiadiazol-2-yl)diazonyl)benzene-1,3-diol.(HL⁴)] were synthesized and characterized by elemental analyses, IR, UV–Vis as well as mass spectroscopy. Cu(II) complexes of the investigated azo dyes have been synthesized and characterized by elemental analyses, IR, electronic and ESR spectra, magnetic susceptibility and thermogravimetric analyses. The bond lengths and bond angles have been calculated to confirm the geometry of the ligands and their Cu(II) complexes. The mode of interaction of the azodyes to copper nanoparticles was described as coordination mode of charged dye molecules on the colloidal Cu⁰ surface through anchoring –OH[−] group. The apparent association constants of the colloidal copper nanoparticles azodye complexes in solution were evaluated using the spectral method and compared with the formation constant of the Cu(II) azo complexes. The antitumor and antioxidant activities of the synthesized azo dyes and their Cu(II) azo complexes have been evaluated.

© 2013 Elsevier B.V. All rights reserved.

Introduction

Metal complexes of azo compounds have remained an attractive area of research for coordination and structural chemists. The importance of the heterocyclic azo dyes may stem from its biological activity and analytical applications [1–6]. Recent years have

a great deal of interest in the synthesis and characterization of azo compounds and their metal complexes [7–13].

Metal complexes of 1,2,4-triazole derivatives are biologically active having nuclease like activity [14], anti-proliferative [15], antibacterial and antifungal activity [16–19], antitumor [20] and anticancer [21]. Also, the chemistry of 1,3,4-thiadiazole derivatives received much attention because of their significant biological activities [22] and anticancer activity [23].

In the present work, we synthesized new four azo dyes compounds (HL¹–HL⁴). The structures of these azo compounds were elucidated by elemental analysis, IR, UV–Vis and mass spectra. The coordination behavior of the investigated azo dyes towards

* Corresponding author. Tel./fax: +20 40 3350804.

E-mail address: abuelazm@yahoo.com (M. Gaber).

¹ Prepared Basic Science, Deanery of Academic Services, Taibah University, Al-Maddinah, Saudi Arabia.

² Faculty of Science and Arts at Al-Rass, Qassim, Saudi Arabia.

Cu(II) ion was studied via the elemental analysis, IR, electronic, ESR spectra, magnetic moment and molar conductance measurements. In addition, the thermal behavior of Cu(II) complexes was studied. The kinetic and thermodynamic parameters for the decomposition steps have been calculated. The mode of interaction between the synthesized azo-compounds and copper nanoparticles in solution was studied. The biological activities (antitumor and antioxidant) of the azo-compounds and their Cu(II) complexes were evaluated.

Experimental

Reagents

All the reagents and solvents were of analytical grade quality. 3-Amino-1H-1,2,4-triazole, 3-amino-5-methylmercapto-1H-1,2,4-triazole, 2-amino-1,3,4-thiadiazole, 2-amino-5-mercapto-1,3,4-thiadiazole, cetyltrimethyl ammonium bromide (CTAB) and 1,3-dihydroxybenzene were purchased from Sigma–Aldrich Co. and were used without further purification.

Physical measurements

Elemental analyses of the azo ligands and their Cu(II) azo complexes were performed with the aid of Perkin–Elmer model 2400 automated analyzer. Infrared spectra for both azo ligands and their Cu(II) azo complexes were recorded on Perkin Elmer 1430 Infrared Spectrophotometer using KBr discs in the range 200–4000 cm^{-1} . Electronic absorption spectra of azo ligands and their Cu(II) azo complexes were recorded in the range 200–700 nm on a Shimadzu Recording UV–Vis spectrophotometer model 240 A with the aid of 1 cm quartz cuvettes. The electronic absorption spectra of the solid Cu(II) azo complexes were recorded using Nujol mull technique [24].

The mass spectra of azo compounds were recorded using Shimadzu Qp-2010 plus. Magnetic susceptibilities of the prepared solid Cu(II) azo complexes were measured at room temperature at 25 °C on Sherwood Scientific Magnetic Susceptibility Balance using $\text{Hg}[\text{Co}(\text{SCN})_4]$ as calibrant. The ESR spectra of powdered samples of Cu(II) azo complexes were recorded at room temperature with the aid of JEOL JES-FE2XG Spectrometer equipped with an E101 micro wave bridge. The magnetic field was calibrated with diphenyl picrylhydrazide (DPPH). The conductance measurements for the prepared solid Cu(II) azo complexes were recorded with the aid of Hana model 1331 conductometer. The thermal analysis (TGA–DrTGA) was performed using Shimadzu TG-50 thermal analyzer up to 800 °C at a heating rate 10 °C min^{-1} in an atmosphere of N_2 . The morphology of the prepared copper nanoparticles was investigated using JEOL-JEM-100SX electron microscope. The particle size and size distributions were obtained by image analyses. The antitumor activity of investigated azo compounds ($\text{HL}^1\text{–HL}^4$) and their Cu(II) azo complexes were evaluated against Ehrlich Ascites Carcinoma cells. Also, the antioxidant assay for some synthesized azo ligand and their Cu(II) azo complexes was performed.

Synthesis of the azo ligands ($\text{HL}^1\text{–HL}^4$) and their Cu(II) azo complexes

Synthesis of azo compounds

Azo dyes ($\text{HL}^1\text{–HL}^4$) Fig. 1, were synthesized by coupling the diazonium salt of 3-Amino-1H-1,2,4-triazole, 3-amino-5-methylmercapto-1H-1,2,4-triazole, 2-amino-1,3,4-thiadiazole, 2-amino-5-mercapto-1,3,4-thiadiazole with 1,3-dihydroxybenzene at -5 to 0 °C. The precipitated solids were filtered off, washed several times with bidistilled water, purified by further recrystallization from hot ethanol to give the pure azo ligands and finally dried in

desiccator over anhydrous CaCl_2 . The analytical and physical data of the synthesized azo compounds were presented in Table 1.

Preparation of Cu(II) azo complexes

The solid Cu(II) azo complexes were prepared in molar ratio 1:1 by dropwise addition of 50 mL hot ethanolic Cu(II) acetate solution (1 mmol) to the azo-compounds (1 mmol) in 50 mL of hot ethanol, whereupon suspensions of the Cu(II) azo complexes resulted. The reaction mixture was then heated at ~ 50 °C under refluxed for 4–5 h. TLC plates were used to detect the reaction finishing. The precipitated solids were collected by filtration, washed several times with bidistilled water and then dried in desiccator over anhydrous CaCl_2 . The analytical and physical data of the synthesized complexes were presented in Table 1.

Synthesis of copper nanoparticles

Cu nanoparticles were synthesized as previously described [20] by reduction of Cu^{+2} to Cu^0 . 10 ml of 0.003 M $\text{Cu}(\text{NO}_3)_2 \cdot 3\text{H}_2\text{O}$ prepared in isopropanol (IPA) solution was added dropwise to 10 ml of 0.09 M of cetyltrimethylammonium bromide/isopropanol (CTAB/IPA) solution. The reaction mixture was stirred vigorously giving a violet colloid absorbing at 560 nm. The appearance of a violet color indicated the presence of copper nanoparticles [25]. CTAB was used as catalyst for the reduction of Cu^{2+} with IPA and as stabilizer to protect Cu nanoparticles from oxidation.

Molecular modeling

An attempt to gain a better insight on the molecular structure of the ligands and their complexes, geometry optimization and conformational analysis has been performed by the use of MM + force-field as implemented in hyperchem 8.0 [26]. Semi empirical method PM3 is then used for optimizing the full geometry of the system using Polak–Ribiere (conjugate gradient) algorithm and Unrestricted Hartree–Fock (UHF) is employed keeping RMS gradient of 0.01 kcal/mol.

Results and discussion

Study of the azo ligands ($\text{HL}^1\text{–HL}^4$)

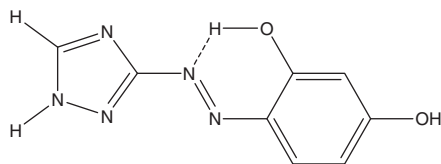
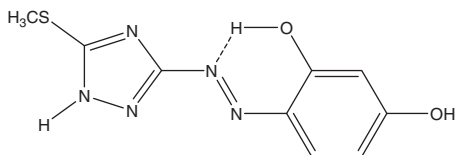
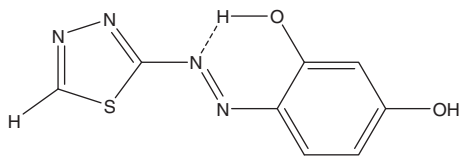
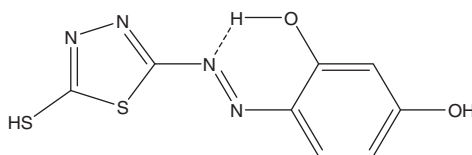
U.V–Vis spectra

The electronic absorption spectra of 5×10^{-5} M azo ligands ($\text{HL}^1\text{–HL}^4$) in methanol showed three main absorption bands. The first band appeared around 210 nm assigned to the moderate energy $\pi\text{--}\pi^*$ electronic transition within the phenyl moiety represented the (${}^1\text{L}_a \rightarrow {}^1\text{A}$) state. The second band observed in the range 250–310 nm attributed to low energy $\pi\text{--}\pi^*$ electronic transition of the heterocyclic moiety and phenyl ring corresponded to the (${}^1\text{L}_b \rightarrow {}^1\text{A}$) state. The third band appeared within the range 380–470 nm derived from n to π^* electronic transition involving the whole electron system and charge transfer interaction within the molecule.

Solvent effect on UV–Vis spectra

The electronic absorption spectra of 10^{-5} M azo ligands ($\text{HL}^1\text{–HL}^4$) under investigation were also recorded in Ethanol, Di-methylformamide, Acetonitrile, Methylene chloride and *n*-Heptane.

The plot of charge transfer energy (E_{CT}) against the solvent parameters such as dielectric constant (\mathbf{D}) given by Suppan [27], refractive index relation $\mathbf{F}(\mathbf{n})$ of Bayliss and Mac Rae, Dimroth and Reichardt's $\mathbf{E}_\text{T}(\mathbf{30})$, Kosower's \mathbf{Z} , Kamlet and Taft's π^* solvatochromic scales, α scale of acidity and β scale of basicity, gave non

(E)-4-((1H-1,2,4-triazol-3-yl)diazenyl)benzene-1,3-diol.(HL¹).(E)-4-((5-(methylthio)-1H-1,2,4-triazol-3-yl)diazenyl)benzene-1,3-diol.(HL²).(E)-4-((1,3,4-thiadiazol-2-yl)diazenyl)benzene-1,3-diol.(HL³).(E)-4-((5-mercapto-1,3,4-thiadiazol-2-yl)diazenyl)benzene-1,3-diol.(HL⁴).**Fig. 1.** Structure of ligands (HL¹–HL⁴).**Table 1**Elemental analysis and physical properties of the prepared azo ligands (HL¹–HL⁴) and their Cu(II) azo complexes.

Ligand/complex	Formula/(mol.wt)	Color	m.p. °C	Content% (calcd.) found			
				%C	%H	%N	%Cu
HL ¹	C ₈ H ₇ N ₅ O ₂ /(205)	Yellow	200	(46.87) 46.8	(3.44) 3.41	(34.16) 34.1	–
[CuHL ¹ (H ₂ O)]·OAc·H ₂ O/362.79		Reddish violet	>300	(33.11) 33.28	(3.6) 3.64	(19.3) 19.22	(17.5)17.31
HL ²	C ₉ H ₉ N ₅ O ₂ S/(251)	Orange	212	(43.07) 43.00	(3.60) 3.51	(27.90) 27.77	–
[CuHL ² (H ₂ O)]·OAc·2H ₂ O/426.9		Reddish violet	>300	(30.90) 30.79	(4.0) 4.1	(16.4) 16.37	(14.89)14.8
HL ³	C ₈ H ₆ N ₄ O ₂ S/(222)	Greenish yellow	237	(43.28) 43.11	(2.70) 2.60	(25.24) 24.98	–
[CuHL ³ (2H ₂ O)]·OAc·H ₂ O/397.9		Reddish violet	>300	(27.9) 27.78	(3.3) 3.21	(13.0) 12.73	(14.8)14.64
HL ⁴	C ₈ H ₆ N ₄ O ₂ S ₂ /(254)	Reddish orange	131	(37.83) 37.70	(2.38) 2.25	(22.06) 21.97	–
[CuHL ⁴ (2H ₂ O)]·OAc·H ₂ O/429.9		Reddish violet	>300	(30.2) 30.11	(3.5) 3.35	(14.1) 13.91	(16.0) 15.0

linear relationships. This indicated that each solvent parameter had its effective contribution to the CT band which depends on the nature of the solute. Accordingly, it can be concluded that the change of the CT band position with solvent was the net result of the influence of all these parameters.

Moreover, the contribution of each solvent parameter in controlling the E_{CT} was calculated. This contribution was calculated for each of Kamlet–Abboud–Taft's three solvent parameters and Katritzky's three solvent parameters. Tables (S1, S2),

From the data one can notice that:

1. The energy of charge transfer band (E_{CT}) for all ligands was solvent dependent.
2. It was clear that, the Kamlet Taft parameters equation has the higher correlation coefficient (0.804–0.994) than Katritzky parameters equation (0.576–0.953) and so, Kamlet Taft equation can be used as indication for the solvatochromic properties for azo ligands (HL¹–HL⁴).
3. The value of contribution of each solvent parameter measured the magnitude of the effect on the energy of charge transfer band. It was found that hetero cyclic moiety in ligands

(HL¹–HL⁴) is responsible for the band shift which appeared from the difference of the contribution results which was $\{\pi^*, \beta\}$ for Kamlet–Abboud–Taft's equation and $\{F(\epsilon), F(n)\}$ for Katritzky's equation.

Mass spectra

The mass spectra of the ligands displayed molecular ions which confirmed their molecular weights (Scheme S1–S4). The mass spectra of ligands showed the molecular ion peak [M⁺] at $m/z = 205$ (80%) with a great abundance equivalent to its molecular mass attributed to C₈H₇N₅O₂ formula for HL¹; at $m/z = 251$ (53%) related to C₉H₉O₂N₅S formula for HL²; at $m/z = 222$ (1%) corresponded to the mass of C₈H₆N₄O₂S formula for HL³ and at $m/z = 254$ (11%) corresponded to C₈H₆N₄S₂O₂ formula with moderate abundant for HL⁴.

IR spectral studies

The IR spectra of the azo compounds (Table S3) showed the characteristic bands due to stretching frequency of the OH group in the region 3329–3427 cm⁻¹. The broadening of this peak indicated that these compounds have strong intramolecular hydrogen bonding O–H...N between the hydroxyl group and the azo nitrogen [28]. A strong band within the region 1247–1297 cm⁻¹ could be attributed to $\nu(C-O)$ vibration of the C–O–H group [29]. In addition, IR spectra of the azo compounds showed an absorption band in the region 1434–1495 cm⁻¹, which assignable to the stretching vibration of (N=N) group. The data obtained from spectral measurements and elemental analyses, confirmed the proposed formula of the investigated azo compounds. The IR spectrum of (HL⁴) showed a band at 2633 cm⁻¹ assigned to $\nu(S-H)$ vibration mode indicating the existence of thiol form. Also, the band appeared at 661 cm⁻¹ is attributed to $\nu(C-SCH_3)$ while the C–S–C stretching vibration appeared at 629 and 633 cm⁻¹ for ligands HL³ and HL⁴, respectively.

Study of Cu(II) azo complexes (1–4) in solution

UV–Vis spectra

The evaluation of the optimum conditions for complexation of Cu(II) ion with azo compounds (HL¹–HL⁴) included a careful investigation of all factors involved in the procedure. The optimum stoichiometry of the colored Cu(II) azo complexes was determined using mole ratio method (MRM) [30], Fig. S1 and continuous variation method (CVM) [31], Fig. S2 as well as conductometric titration method (CM). All the previous methods were agree with the stoichiometry of 1:1 (M:L) complexes. The stability constants of Cu(II) azo complexes were determined by the aid of the data obtained from (MRM) and (CVM) applying the Harvey and Manning equation [32], Table 2. The conductometric method (CM) showed that the conductance increased with increasing the addition of ligand. This indicated that the reaction between Cu(II) ion and azo occurred via the formation of a covalent linkage with oxygen of the phenolic OH group, i.e. the conductance increases due to the liberation of H⁺ ion.

The limits of Cu(II) ion concentration at which the M–L system obeyed Beer's law, molar absorptivity, Sandell sensitivity, Standard deviation and Correlation coefficient were listed in Table 2. These values confirmed the possible application of the present spectrophotometric method for the determination of Cu(II) ion. Ringbom [33] concentration range was also determined and the results were listed in Table 2. The obedience to Beer's law and Ringbom plots of Cu(II) complexes were shown in Figs. (S3, S4).

The spectrophotometric titration of Cu(II) ion with EDTA using the azo compounds (HL¹–HL⁴) were carried out. The titration curves shown in Fig. 2. exhibited the presence of two intersected straight lines. The point of intersection indicated the end point

Table 2

Spectrophotometric data, stability constants and analytical data (Molar absorptivity (ϵ), specific absorptivity (a), Sandell sensitivity (S), Standard deviation (S.D.), correlation coefficient (C.C.) and obedience of Beer's law for Cu(II) with (HL¹–HL⁴).

Data	Complex 1	Complex 2	Complex 3	Complex 4
λ_{max} (nm)	510	540	460	550
Beer's range (ppm)	0–3.175	0–3.81	0–3.175	0–6.35
Ringbom range (ppm)	0.281–	0.212–	0.173–	0.344–
	0.58	0.58	0.50	0.80
CC	0.99383	0.99439	0.99788	0.995
S.D.	0.00971	0.01851	0.01253	0.00691
ϵ (l mol ⁻¹ cm ⁻¹)	5.6×10^3	8.7×10^3	8×10^3	1.9×10^3
a (ml g ⁻¹ cm ⁻¹)	0.088	0.14	0.126	0.03
S (μ g cm ⁻²)	0.011	0.007	0.008	0.033
MRM	1:1	1:1	1:1	1:1
CVM	1:1	1:1	1:1	1:1
CM	1:1	1:1	1:1	1:1
Log β_n	5.18	3.67	4.69	5.32
$-\Delta G^\circ$	7062.5	5003.8	6394.4	7253.4
$Y \times 10^{-5}$	5	5	5	5
$X \times 10^{-5}$	5	5	5.1	5
K (bulk-copper)	12765	10566	4752	3915
K (nano-copper)	85E + 8	53E + 8	46E + 8	20E + 8

Where: MRM: mole ratio method. CVM: continuous variation method. CM: conductometric method. β_n : stability constant of complex. X: concentration of prepared sample (mol L⁻¹). "EDTA-titration". Y: concentration of sample (mol L⁻¹) calculated experimentally. "EDTA-titration". ΔG° : Gibbs free energy change (Cal mol⁻¹). (K): Formation constant of Cu(II) azo complexes. (K_{app}): Apparent association constant of Cu⁰ azo complexes.

for the titration process of the Cu(II) ion with EDTA as a standard solution using (HL¹–HL⁴) as indicators. The results indicated that the Cu(II) ion was successfully determined up to the range listed in Table 2. The results obtained indicated that the applied ligands can be used as indicators for the spectrophotometric titration of the Cu(II) with EDTA.

Stability constant measurement

The addition of different concentration of Cu(II) acetate to azo ligands (HL¹–HL⁴) were studied, where a new absorption band appeared at 510, 540, 460 and 550 nm related to the complex formation of Cu(II) with HL¹, HL², HL³ and HL⁴, respectively. The formation constant of the complexes was estimated from Benesi and Hildebrand equation [34]

$$\frac{[L_0]}{A - A_0} = \frac{1}{\epsilon_{ML} - \epsilon_L} + \frac{1}{(\epsilon_{ML} - \epsilon_L)K[M_0]}$$

where, A_0 and A are absorbance of the free azo ligand solutions and the corresponding Cu(II) azo complexes, respectively, at a given

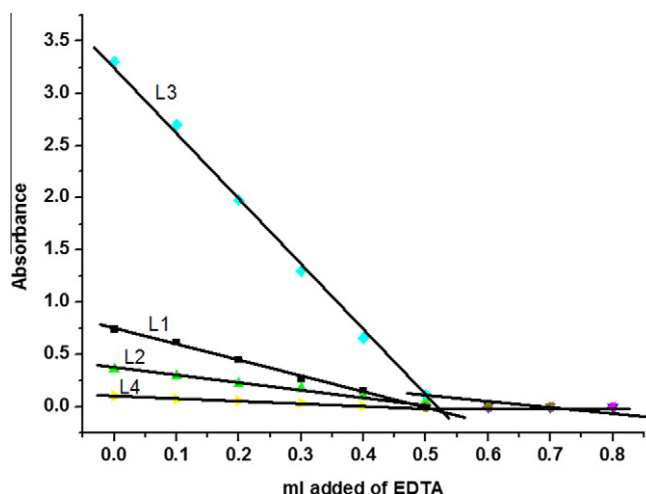


Fig. 2. Spectrophotometric titration of Cu(II) with EDTA using azo ligands (HL¹–HL⁴) as indicators.

wavelength; ϵ_L and ϵ_{ML} are the molar extinction coefficients of the azo ligands and their Cu(II) azo complexes, respectively; $[L_0]$ is the initial concentration of azo ligands and finally $[M_0]$ is the Cu(II) concentration. Formation constant (K) values, correlation coefficient and standard deviation for the complexes of azo ligands (HL¹–HL⁴) with Cu(II) ion were calculated from the plots of $[L_0]/(A-A_0)$ versus $1/[M_0]$, Fig. (S5) and values were listed in Table 2. The results obtained revealed that the Cu(II) complexes of the triazole azocompounds were more stable than those of thiadiazole ones due to the formation of two rings giving stability larger than one ring, which give a great evidence to the proposal structure of the prepared complexes.

Coordination with colloidal copper nanoparticles

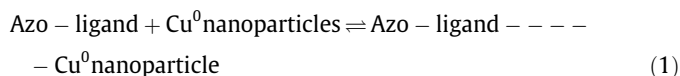
The interaction between azo ligands (HL¹–HL⁴) and colloidal Copper Nanoparticles

The interaction between azo ligands (HL¹–HL³) and copper nanoparticles may occurred through the free anchoring (–OH) group as a result of contribution of the other group in intermolecular hydrogen bond with nitrogen atom of azo group besides the great steric hindrance with hetero ring. Furthermore, for (HL⁴) the interaction occurred through the thiol and hydroxyl groups, Scheme 1.

Absorption characteristics of azo–Cu nanoparticles

Fig. 3. showed the absorption spectrum of azo ligand (HL¹) in the absence and presence of different concentrations of colloidal Cu⁰ nanoparticles. As the the concentration of colloidal Cu⁰ nanoparticles increased, the absorption of azo ligand decreased regularly with appearance of new peak due to the formation of surface complex to a limits in which the Cu⁰ surface was saturated with ligand molecules and up this concentration there was no observed increasing in absorption spectra (Fig. S6) for TEM image for the complex formation [35].

The apparent association constant (K_{app}) for the complex between azo ligand and colloidal Cu⁰ nanoparticles can be given by the equation:



$$K_{app} = \frac{[\text{Azo} - \text{ligand} \dots \text{Cu}^0 \text{ nanoparticles}]}{[\text{Azo} - \text{ligand}] \cdot [\text{Cu}^0 \text{ nanoparticles}]}$$

The change in intensity of the absorption peak due to the formation of the surface complex was utilized to obtain K_{app} according to Benesi and Hildebrand.¹¹

$$A_{obs} = (1 - \alpha)C_0\epsilon_{azo-ligand} + \alpha C_0\epsilon_{complex} \quad (2)$$

where A_{obs} is the observed absorbance of the solution containing different concentrations of colloidal Cu⁰ nanoparticles, α is the degree of association between azo ligand and Cu⁰ nanoparticles, $\epsilon_{azo-ligand}$ and $\epsilon_{complex}$ are the molar extinction coefficients at the defined wavelength of azo ligand and the formed complex, respectively. In water, Eq. (2) can be expressed as Eq. (3), where A_0 and A_c are the absorbance of azo ligand and the complex, respectively, with a concentration of C_0 :

$$A_{obs} = (1 - \alpha)A_0 + \alpha A_c \quad (3)$$

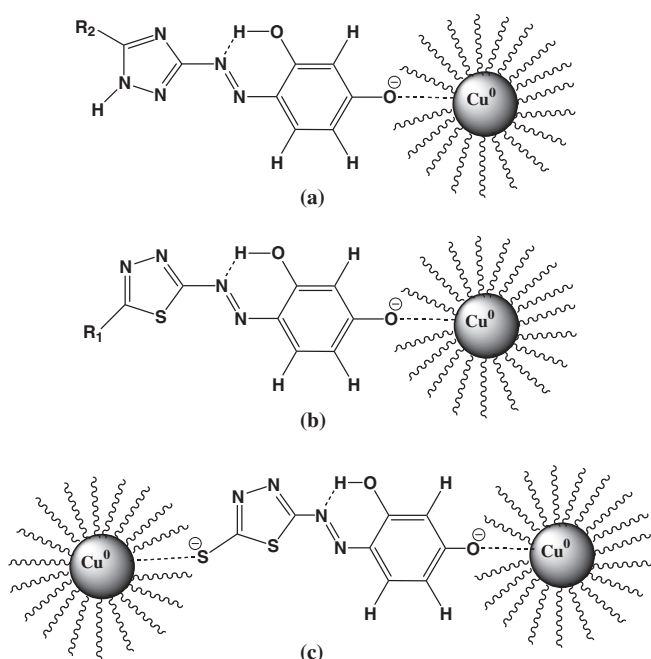
At relatively high Cu⁰ nanoparticles concentrations, α can be equated to $(K_{app}[\text{Cu}^0 \text{ nanoparticles}])/(1 + K_{app}[\text{Cu}^0 \text{ nanoparticles}])$. In this case, Eq. (3) can be changed to Eq. (4):

$$\frac{1}{A_{obs} - A_0} = \frac{1}{A_c - A_0} + \frac{1}{K_{app}(A_c - A_0)[\text{Cu}^0 \text{ nanoparticles}]} \quad (4)$$

The enhancement of absorbance was due to absorption of the surface complex, i.e. donor–acceptor behavior [36,37] based on the good linear relationship between $1/(A_{obs}-A_0)$ versus reciprocal concentration of colloidal Cu⁰ nanoparticles with a slope equal to $1/K_{app}(A_c-A_0)$ and an intercept equal to $1/(A_c-A_0)$ Fig. 4. The correlation coefficient, standard deviation and values of the apparent association constant (K_{app}) were determine from this plot. Further, the reason for the highest apparent association constant of Cu⁰ nanoparticles compared to that bulk copper may be due to the larger surface area of the Cu⁰ nanoparticles.

Studies of the solid complexes (C₁–C₄)

The azo compounds reacted with Cu(II) acetate·4H₂O in 1:1 mol ratio leading to the formation of complexes having the general formula $[\text{CuHL}^{1-4}(x\text{H}_2\text{O})]\cdot\text{OAc}\cdot y\text{H}_2\text{O}$, Table 1. The isolated solid



Scheme 1. The mode of interaction between (a) HL¹, HL². (b) HL³ and (c) HL⁴ with the surface of colloidal Cu⁰.

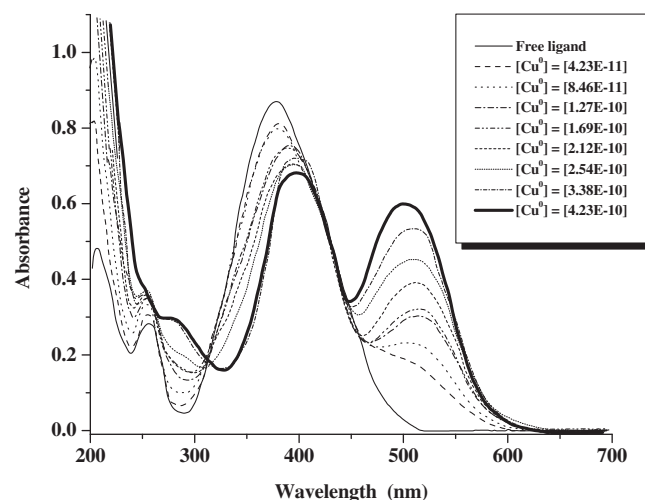


Fig. 3. Showed the absorption spectrum of azo ligand (HL¹) in the absence and presence of different concentrations of colloidal Cu⁰ nanoparticles.

complexes were stable and insoluble in common organic solvents but soluble in DMF and DMSO. The solid Cu(II) azo complexes were subjected to elemental analyses, spectral, conductance, magnetic measurements as well as thermal analysis. The elemental analyses were in agreement with the formula suggested in Table 1 and Scheme 2.

Conductivity measurement

The molar conductance values of the isolated complexes measured in DMF solution (10^{-3} M) at room temperature are 80, 100, 90 and $110 \Omega^{-1} \text{ mol}^{-1} \text{ cm}^2$ for Cu(II) complexes C₁, C₂, C₃ and C₄, respectively, indicating the ionic nature of the complexes [38]. Also, the addition of FeCl₃ solution to the solution of complexes gave the reddish brown coloration confirming the non coordination of acetate anion, i.e. acetate anion was outside the coordination sphere.

IR spectra

The infrared spectra of the solid Cu(II) azo complexes displayed interesting changes that may give a reasonable idea about the structure of the metal complexes, (Table S3)

- All complexes showed a broad band in the range $3330\text{--}3420 \text{ cm}^{-1}$ assigned to $\nu(\text{OH})$ of the coordination water molecules associated with the complexes.
- The $\nu(\text{N}=\text{N})$ of the free azo compounds exhibited a shift to lower values on complex formation indicating the coordination of the azo nitrogen to the Cu(II) ion, which was supported by the appearance of a new band within the range $444\text{--}486 \text{ cm}^{-1}$ due to M–N bond formation.
- For complexes C₁ and C₂, the $\nu(\text{C}=\text{N})$ group of the triazole ring was shifted to lower wavenumbers indicating the participation of azomethine nitrogen atom on complex formation. For Cu(II) complexes C₃ and C₄, $\nu(\text{C}=\text{N})$ remained unchanged indicating that the (C=N) group of the thiadiazole ring was not involved in the coordination.
- The phenolic (C–O) stretching vibration of the free azo compounds was shifted to higher values by $25\text{--}85 \text{ cm}^{-1}$ indicating the involvement of the phenolic oxygen in complex formation.
- The appearance of a new band in the spectra of Cu(II) complexes within the range $532\text{--}583 \text{ cm}^{-1}$ which may be assigned to M–O bond.
- The appearance of new bands at $3420, 1610, 940$ and 630 cm^{-1} due to $\nu(\text{OH}), \delta(\text{H}_2\text{O}), \rho_{\text{rock}}(\text{H}_2\text{O})$ and $\rho_{\text{wagg}}(\text{H}_2\text{O})$, respectively, corresponding to coordination water.

From the above arguments together with the elemental analyses, it was concluded that the azo compounds (HL¹, HL²) behave as mono-negative tridentate ligands with ONN donor sites while azo compounds (HL³, HL⁴) behave as mono-negative bidentate ligands with ON donor sites.

Electronic spectra and magnetic measurements

The electronic absorption spectra of Cu(II) azo complexes (C₁ and C₂) exhibited two bands at (14925, 18667) and (15152, 17857) cm^{-1} attributed to ${}^2\text{B}_{1g} \rightarrow {}^2\text{A}_{1g}$ and ${}^2\text{B}_{1g} \rightarrow {}^2\text{E}_{1g}$ transitions which favored square planar geometry around Cu(II) ion [39]. The electronic spectra of Cu(II) azo complexes (C₃ and C₄) exhibited characteristic band at 16949 and 16129 cm^{-1} corresponding to the tetrahedral geometry. Cu(II) complexes (C₁–C₄) have normal magnetic moments values (1.75–1.87 BM) corresponding to the mono-nuclear Cu(II) complexes [8].

ESR spectra

The ESR spectra of the powdered Cu(II) azo complexes (C₁–C₄) were recorded at room temperature (25 °C) and the g-values are listed in Table 3. The ESR spectra of complexes were characteristic of a monomeric configuration and having an axial symmetry type of $d_{x^2-y^2}$ ground state which is most common for Cu(II) complexes.

The ESR spectra of Cu(II) azo complexes exhibited two g-values. The g-values of all complexes have a positive contribution from the value of the free electron (2.0023) due to the measurable covalent character in the bonding between the azo ligands and Cu(II) ion. The values of $g_{11} < 2.3$ indicating that the Cu(II)-azo compounds bonds have the covalent character [40]. Also, the g values are related by the expression $G = (g_{11} - 2)/(g_{\perp} - 2)$. If the value of $G > 4$, the exchange interaction is negligible whereas if $G < 4$, a considerable exchange interaction is indicated in the solid complexes. The G values of Cu(II) azo complexes were higher than 4 indicated that there was no interaction between Cu centers. The g-values of Cu(II) azo complexes with a ${}^2\text{B}_{1g}$ ground state ($g_{11} > g_{\perp}$) may be expressed [41] by:

$$K_{11}^2 = (g_{11} - 2.0023)A_2/8\lambda$$

$$k_{\perp}^2 = (g_{\perp} - 2.0023)A_1/2\lambda$$

$$k^2 = [k_{11}^2 + 2k_{\perp}^2]/3$$

where k_{11}^2 and k_{\perp}^2 were the parallel and perpendicular components, respectively, of the orbital reduction factor k , λ was the spin-orbit coupling constant (-828 cm^{-1}) for free copper, A_1 and A_2 were the electronic transition ${}^2\text{B}_{1g} \rightarrow {}^2\text{E}_{1g}$ and ${}^2\text{B}_{1g} \rightarrow {}^2\text{B}_{2g}$ respectively, the calculated values of k_{11}^2, k_{\perp}^2 indicated that $k_{11} < k_{\perp}$ which was a good evidence for the assumed ${}^2\text{B}_{1g}$ ground state. The lower values of k than unity were indicative of their covalent nature which in agreement with the conclusion obtained from the values of g_{11} . Significant information about the nature of bonding in Cu complex can be derived from the relative magnitudes of k_{11} and k_{\perp} . In case of pure σ -bonding, $k_{11} \sim k_{\perp} \sim 0.77$, whereas $k_{11} < k_{\perp}$ implies considerable in-plane π bonding while for out-of-plane π bonding, $k_{11} > k_{\perp}$. For the Cu(II) complexes under investigation, $k_{11} < k_{\perp}$, implying a greater contribution from in-plane π bonding than from out-of-plane π bonding in metal ligand π bonding [42].

Thermal analysis

Thermogravimetric analyses. The TGA as well as DrTGA data of the thermal decomposition of the Cu(II) azo complexes (C₁–C₄) were listed in Table 4. As an example, the TG curve of C₁ is shown in Fig. S7. The correlation between the different decomposition steps of the complexes with the corresponding weight losses discussed in term of the proposal formula of the complexes as follows:

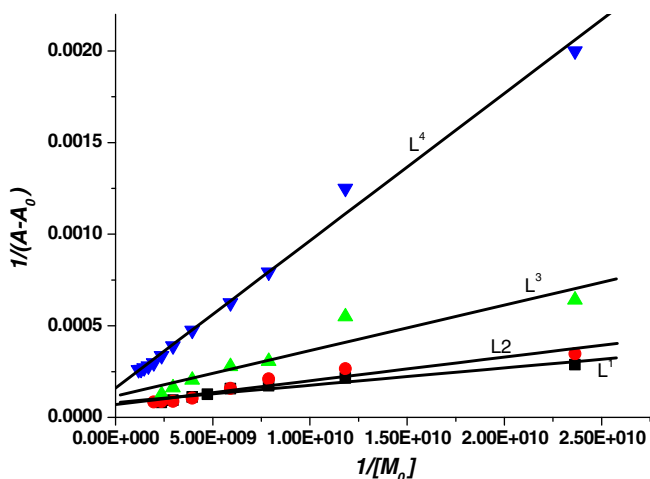


Fig. 4. Linear dependence of $1/(A-A_0)$ on the reciprocal concentration of colloidal copper nanoparticles according to Benesi and Hildebrand equation.

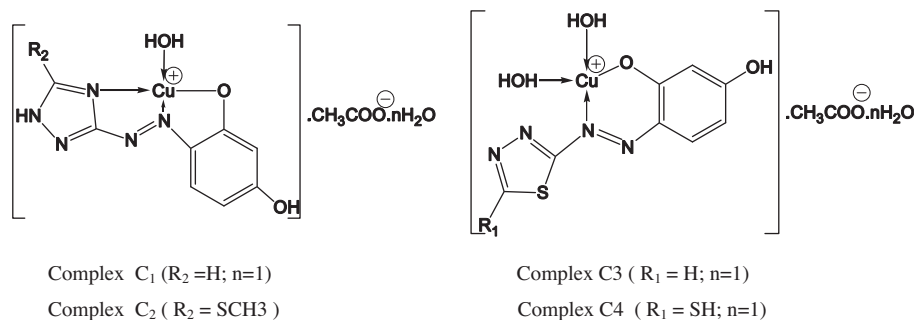
Scheme 2. Structure of complexes (C₁–C₄).

Table 3
Spin hamiltonian and bonding parameters of Cu(II) azo complexes (C₁–C₄).

State	C ₁	C ₂	C ₄
g_{11}	2.244	2.110	2.40
g_{\perp}	2.061	2.026	2.06
g_{av}	2.124	2.054	2.173
G	4	4.23	6.66
k_{11}	0.813	0.80	–
k_{\perp}	0.8897	0.8897	–

- C₁ was thermally decomposed within the temperature range 25–800 °C at successive four degradation steps. The first step within the temperature range 39–92 °C with an estimated mass loss of 4.96% (calcd. 5.03%) corresponded to the loss of one molecule of lattice water. The activation energy of this step is 58.5 kJ/mol. The second degradation step within the temperature range 92–141 °C with an estimated mass loss of 5.22% (calcd. 5.17%) can be assigned to the loss of one molecule of coordination water molecule. The activation energy of this step is 74.6 kJ/mol. The third degradation step within the temperature range 141–444 °C with an estimated mass loss of 20.52% (calcd. 20.49%) corresponded to the loss of hetero ring. The activation energy of this step is 9.3 kJ/mol. The fourth degradation step within the temperature range 444–664 °C with an estimated mass loss of 47% (calcd. 48%) can be assigned to the loss of N₂ gas, acetate and C₆H₄O with the formation of CuO as a final product. The activation energy of this step is 147.5 kJ/mol
- C₂ was thermally decomposed within the temperature range 25–800 °C at successive four degradation steps. The first degradation step within the temperature range 53–148 °C with an estimated mass loss of 8.44% (calcd. 8.43%) corresponded to the loss of two molecules of lattice water. The activation energy of this step is 27.8 kJ/mol. The second degradation step within the temperature range 148–217 °C with an estimated mass loss of 4.61% (calcd. 4.41%) was assigned to the loss of two molecules of coordination water. The activation energy of this step is 109.1 kJ/mol. The third degradation step within the temperature range 217–342 °C with an estimated mass loss of 30.62% (calcd. 30.55%) corresponded to the loss of hetero ring. The activation energy of this step was 52.8 kJ/mol. The fourth degradation step within the temperature range 342–474 °C with an estimated mass loss of 50.66% (calcd. 50.76%) was assigned to the loss of N₂ gas, acetate and C₆H₄O with the formation of CuO as a final product. The activation energy of this step is 562.6 kJ/mol.
- C₃ was thermally decomposed within the temperature range 25–800 °C at successive four degradation steps. The first degradation step within the temperature range 50–133 °C with an estimated mass loss of 4.74% (calcd. 4.73%) corresponded to the loss of one molecule of lattice water. The activation energy

of this step is 23.8 kJ/mol. The second degradation step within the temperature range 133–221 °C with an estimated mass loss of 4.98% (calcd. 4.84%) was assigned to the loss of two molecules of coordination water. The activation energy of this step is 49.25 kJ/mol. The third degradation step within the temperature range 221–335 °C with an estimated mass loss of 17.26% (calcd. 17.29%) corresponded to the loss of acetate molecule. The activation energy of this step is 49.34 kJ/mol. The fourth degradation step within the temperature range 335–461 °C with an estimated mass loss of 51.2% (calcd. 51.27%) was assigned to the loss of N₂ gas, hetero ring and C₆H₄O with the formation of CuO as a final product. The activation energy of this step is 98.7 kJ/mol.

- C₄ was thermally decomposed within the temperature range 25–800 °C at successive four degradation steps. The first dehydration step within the temperature range 38–111 °C with an estimated mass loss of 4.37% (calcd. 4.71%) corresponded to the loss of one molecule of lattice water. The activation energy of this step is 52.6 kJ/mol. The second degradation step within the temperature range 111–187 °C with an estimated mass loss of 4.58% (calcd. 4.61%) corresponded to the loss of two molecules of coordination water. The activation energy of this step is 32.4 kJ/mol. The third degradation step within the temperature range 187–380 °C with an estimated mass loss of 31.25% (calcd. 31.26%) corresponded to the loss of hetero ring. The activation energy of this step is 39.4 kJ/mol. The fourth degradation step within the temperature range 380–667 °C with an estimated mass loss of 49.85% (calcd. 49.85%) was assigned to the loss of N₂ gas, acetate and C₆H₄O with the formation of CuO as a final product. The activation energy of this step is 30.2 kJ/mol

The thermal analysis of Cu(II) complexes confirmed the composition of the complexes and allow the number and the nature of the water molecules determination. Complex C₄ loss coordination water at temperature lower than complex C₃. Also, complex C₁ loss coordination water at lower temperature than complex C₂. The fact that the activation energy of the second step of decomposition is greater than that of the first step may be due to the less steric strain occurring at that point [43].

Kinetic and thermodynamic studies. The kinetic parameters of activation energy (E), reaction order (n) and Arrhenius pre-exponential factor (A) were calculated from the integral method proposed by Coats–Redfern [44] and the approximation method proposed by Horowitz–Metzger [45], Fig. 5. The data listed in Table 5 showed that the values obtained by approximation method were different from those calculated by integral method due to the different mathematical treatment of the obtained data [46].

The selection of the mechanism which best describes the thermal decomposition of the desired complexes was deduced using

Table 4
Thermo analytical results (TGA and DrTGA) of Cu(II) azo complexes (C₁–C₄).

Complex	(TGA)			
	Step	Temperature (°C)	Wt.%loss (calcd.)/found	Assignment
[CuHL ¹ (H ₂ O)]·OAc·H ₂ O	1st	39.89–92.04	(4.96)/5.03	Loss of lattice water
	2nd	92.04–140.62	(5.22)/5.17	Loss of coordination water
	3rd	140.62–444	(20.52)/20.49	Loss of hetero ring
	4th	444–663.7	(47)/47.4	Loss of N ₂ , C ₆ H ₄ O and acetate
[CuHL ² (H ₂ O)]·OAc·2H ₂ O	1st	53.23–147.9	(8.44)/8.43	Loss of two molecules of lattice water
	2nd	147.9–217.11	(4.61)/4.41	Loss of coordination water
	3rd	217.11–342.44	(30.62)/30.55	Loss of hetero ring
	4th	342.44–473.5	(50.6)/50.7	Loss of N ₂ , C ₆ H ₄ O and acetate
[CuHL ³ (2H ₂ O)]·OAc·H ₂ O	1st	49.6–132.5	(4.74)/4.73	Loss of lattice water
	2nd	132.5–220.9	(4.98)/4.84	Loss of two molecules of coordinated water
	3rd	220.9–334.9	(17.16)/17.29	Loss of acetate
	4th	334.9–460.6	(52.1)/52.17	Loss of N ₂ , C ₆ H ₄ O and hetero ring
[CuHL ⁴ (2H ₂ O)]·OAc·H ₂ O	1st	38.3–110.5	(4.37)/4.71	Loss of lattice water
	2nd	110.5–186.6	(4.58)/4.61	Loss of two molecules of coordinated water
	3rd	186.61–379.63	(31.25)/31.26	Loss of hetero ring
	4th	379.63–667.2	(50.66)/50.66	Loss of N ₂ , C ₆ H ₄ O and acetate

the method proposed by the integral method (Coats–Redfern) according to equation:

$$\ln[g(\alpha)/T^2] = \ln(AR/QE) - E/RT$$

$g(\alpha)$ suggested by Satava [47] were used to enunciate the mechanism of thermal decomposition in each stage see Table (S4):

where Q is the heating rate, α is the fraction decomposed, A is Arrhenius pre-exponential factor, R is the universal gas constant, T is the absolute temperature, $g(\alpha)$ is the kinetic model and E is the activation energy.

The quantity $\ln[g(\alpha)/T^2]$ was plotted as a function of $(1000/T)$. The correlation coefficients for nine forms were calculated and the form of $g(\alpha)$ for which the correlation has a maximum value was chosen as the mechanism of reaction. The thermodynamic parameters of activation ΔH^* , ΔS^* and ΔG^* were estimated according to the previous methods with the aid of the following expressions:-

$$\Delta H^* = E - RT$$

$$\Delta S^* = R \ln(hA/K_B T)$$

$$\Delta G^* = \Delta H^* - T\Delta S^*$$

where ΔH^* is the activation enthalpy (kJ mol^{-1}), ΔS^* is the activation entropy ($\text{J mol}^{-1} \text{K}^{-1}$), ΔG^* is the Gibbs activation free energy (kJ mol^{-1}), h is the Plank constant, K_B is the Boltzmann constant and T is the ob-

served peak temperature. The thermodynamic parameters corresponding to each chosen function form were listed in Table 6.

According to the data obtained, the following remarks can be pointed out:

- The high values of the energy of activation of the complexes (ΔE^*) reflect the high stability of the investigating complexes due to their covalent character [48]. The positive sign of ΔG^* for the Cu(II) azo complexes under investigation revealed that the free energy of the final residue is higher than that of the initial compound and all the decomposition steps are non-spontaneous processes.

The values of ΔG^* increased for the subsequent decomposition stages of a given complex. Increasing the values of ΔG^* of a given complex reflected that the rate of removal of the subsequent ligand was lower than that of the precedent ligand, this is due to increasing in the values of $T\Delta S^*$ from one step to another which overrides the values of ΔH^* [49].

- The negative values of ΔS^* indicated a more order activated complex than reactant and/or the reaction was slow [50].
- The positive values of ΔH^* means that the decomposition processes were endothermic.

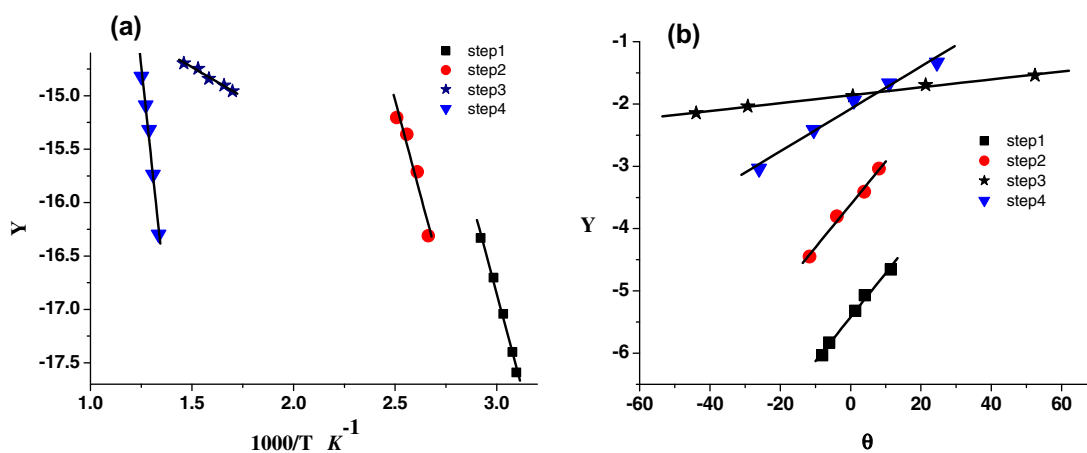


Fig. 5. (a) Plotting $Y = \log(-\log(1-\alpha)/T^2)$ versus $1000/T$ (K^{-1}) for $n = 1$ and $Y = \log(1-(1-\alpha)^{1-n}/T^2(1-n^2))$ versus $1000/T$ (K^{-1}) for $n \neq 1$ for the different decomposition steps of complex C₁ using Coats–Redfern equation. (b) Plotting $Y = \log(1-(1-\alpha)/T^2)$ versus θ for $n = 1$ and $Y = \log(1-(1-\alpha)^{1-n}/T^2(1-n^2))$ versus θ for $n \neq 1$ for the different decomposition steps of complex C₁ using Horowitz–Metzger equation.

Table 5Kinetic parameters of activation for complexes (C₁–C₄) using Coats–Redfern (CR) and Horowitz–Metzger (HM) methods.

Complex	Step	Method	n	r	E	A
C ₁	1st	CR	1	0.9840	58.49	974.9571
		HM	2	0.9967	64.44	46529943
	2nd	CR	1	0.9905	74.59	43.721
		HM	2	0.9905	81.69	1882421
	3rd	CR	1	0.9922	9.25	5.24E + 09
		HM	2	0.9972	21.14	0.552203
	4th	CR	1	0.9922	147.49	102.4779
		HM	2	0.9927	170.08	1.25E + 10
C ₂	1st	CR	0	0.9923	27.78	11116286
		HM	0	0.9953	33.36	803.5078
	2nd	CR	1	0.9995	109.14	0.80649
		HM	2	0.9890	119.20	3.18E + 11
	3rd	CR	1	0.9874	52.85	1501931
		HM	2	0.9889	67.68	84353.55
	4th	CR	0	0.9896	562.61	1.28E - 34
		HM	0	0.9898	573.92	3.24E + 46
C ₃	1st	CR	0	0.99981	23.48	71666998
		HM	0	0.98718	29.16	89.41566
	2nd	CR	1	0.9963	49.25	1620272
		HM	2	0.9953	57.65	22172.16
	3rd	CR	0	0.9938	49.34	10753305
		HM	0	0.9963	58.57	2855.612
	4th	CR	1	0.9929	98.70	2373.113
		HM	2	0.9911	113.76	1.25E + 08
C ₄	1st	CR	1	0.9973	52.56	5830.452
		HM	3	0.9970	58.94	7137804
	2nd	CR	1	0.9965	32.42	33583537
		HM	2	0.9970	40.87	607.998
	3rd	CR	1	0.9886	39.41	31620512
		HM	2	0.9829	50.68	933.7278
	4th	CR	1	0.9925	30.24	5.67E + 08
		HM	0.5	0.9893	39.94	9.470626

Molecular modeling

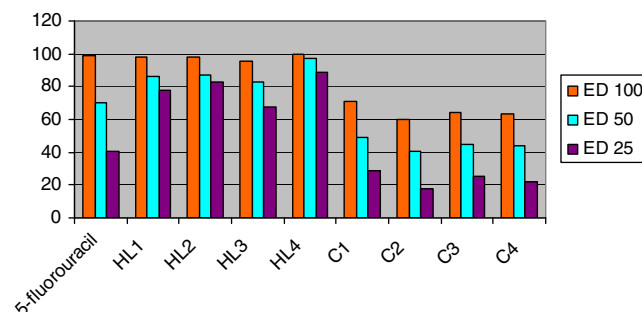
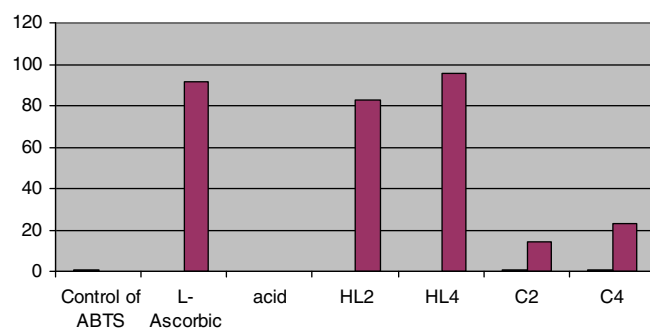
The molecular structure along with atom numbering of the ligands and complexes are shown in structures (1–8). Data analysis in Tables S5–S12 (Supplementary material) for bond lengths and bond angles of the ligands and their complexes revealed the following remarks:

1. The N=N bond length is elongated due to the formation of Cu–N bond. The same trend was observed for the C=N bond length of the hetero ring [51].

Table 6Integral methods and their corresponding thermodynamic parameters for Cu(II) azo complexes (C₁–C₄).

No.	Complex	Step	g(α)	r	Thermodynamic parameters				
					ΔE*	ΔH*	A	–ΔS*	ΔG*
C ₁	[CuHL ¹ (H ₂ O)].OAc.H ₂ O	1st	[1–(1–α) ^{1/3}] ²	0.98542	122.40	119.64	1.52E + 09	0.070	142.82
		2nd	[1–(1–α) ^{1/3}] ²	0.99118	155.01	151.82	1.97E + 12	0.012	156.28
		3rd	[1–(1–α) ^{1/3}] ²	0.99683	28.06	22.81	1.06E - 07	0.385	266.02
		4th	[1–(1–α) ^{1/3}] ²	0.99236	301.68	295.24	4.8E + 12	0.010	303.18
C ₂	[CuHL ² (H ₂ O)].OAc.2H ₂ O	1st	α ²	0.99366	60.47	57.56	4.46	0.234	139.54
		2nd	[1–(1–α) ^{1/3}] ²	0.99951	225.38	221.55	3.25E + 16	0.068	252.63
		3rd	[1–(1–α) ^{1/3}] ²	0.99190	46.99	42.29	4.4E - 5	0.334	230.85
		4th	α ²	0.98976	1135.55	1130.38	1.35E + 88	0.436	2023.36
C ₃	[CuHL ³ (2H ₂ O)].OAc.H ₂ O	1st	α ²	0.99984	52.96	49.96	0.09	0.267	146.30
		2nd	[1–(1–α) ^{1/3}] ²	0.99679	105.78	101.91	369.40	0.199	194.69
		3rd	α ²	0.99468	107.88	103.28	106.12	0.211	220.167
		4th	[1–(1–α) ^{1/3}] ²	0.98907	192.84	187.53	1.91E + 08	0.093	246.73
C ₄	[CuHL ⁴ (2H ₂ O)].OAc.H ₂ O	1st	[1–(1–α) ^{1/3}] ²	0.99760	110.57	107.70	27108733	0.104	143.46
		2nd	[1–(1–α) ^{1/3}] ²	0.99713	71.58	68.03	0.16	0.263	180.60
		3rd	[1–(1–α) ^{1/3}] ²	0.98892	80.03	75.06	0.08	0.272	237.56
		4th	[1–(1–α) ^{1/3}] ²	0.99313	66.89	60.01	0.0003	0.322	326.55

Where ΔE*, ΔH* and ΔG* in kJ mol⁻¹ while ΔS* in J mol⁻¹ K⁻¹ and A in S⁻¹.

**Fig. 6.** In vitro cytotoxicity of azo ligands (HL¹–HL⁴) and their Cu(II) azo complexes (C₁–C₄) on EAC compared to 5-fluorouracil.**Fig. 7.** Antioxidant assay for azo ligand (HL², HL⁴) and their Cu(II) azocomplexes.

- There is a variation in C–O bond lengths on complexation. It becomes slightly longer (for complexes C₁ and C₂) or shorter (for complexes C₃ and C₄) as the coordination takes place via o-atom of C–O group that is formed on deprotonation of C–OH leading to the formation of Cu–O bond [52].
- The bond length of Cu–O increases in the order C₁ > C₂ > C₃ > C₄ while Cu–N increases in the order C₁ > C₂ > C₄ > C₃.
- The bond angles around the N=N group were reduced upon coordination.

5. The bond angle in Cu(II) complexes C_1 and C_2 lie in the range reported for square planar geometry while for complexes C_3 and C_4 the bond angle are quite near to the tetrahedral geometry.

Biological activities

In vitro antitumor activity

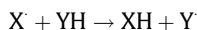
Antitumor activity of the investigated azo ligands (HL¹–HL⁴) and their Cu(II) azo complexes (C_1 – C_4) were evaluated against Ehrlich Ascites Carcinoma (EAC) derived from ascetic fluid of the female Swiss albino mice (purchased from National Cancer Institute, Cairo, Egypt) after 2 weeks of their injection with 1×10^6 EAC. Different concentrations of the tested compounds dissolved in DMSO were prepared (100, 50 and 25 μ l/ml from 1 mg/ml in DMSO) then 0.1 ml of each concentration was added to the suspension of tumor cells which was then cultured in round bottom 96-well plate for 2 h at 37 °C in humidified atmosphere with 5% CO₂. The same volume of DMSO was added to some wells as control. 5-fluorouracil was used as a standard cytotoxic agent. The viability of the cells was determined under microscopical examination using hemocytometer after staining with trypan blue. In this assay, blue cells absorb the dye and appear blue while the viable cells appear unstained. The data are summarized in Table (S13) and illustrated in Fig. 6.

By comparing the cytotoxicity of the investigated compounds, it was found that

- All Cu(II) azo complexes expressed less cytotoxic than their free azo ligands which may be a result of coordination and
- The highest cytotoxic effects of HL⁴ at its lowest dose (ED25) as shown in Table S13 could be attributed to its high sulphur atom number as well as to its high anti-oxidant effects as shown in Fig. 7 and Table S14.

ABTS antioxidant activity screening

The antioxidant activity assay employed here is one of the several assays that depend on measuring the consumption of stable free radicals. The methodology assumes that the consumption of the stable free radical (X[•]) will be determined by reactions as follows:



The rate and/or the extent of the process measured in terms of the decrease in X[•] concentration would be related to the ability of the added compounds to trap free radicals. The absorbance was measured at a specific wavelength and the reduction in color intensity of the free radical solution due to scavenging of the free radical by the antioxidant was expressed as inhibition percentage. The assay employs the radical action derived from

2,2-azino-bis(3-ethyl benzthiazoline-6-sulfonic acid) (ABTS) as stable free radical to assess antioxidant potential of the investigating compounds.

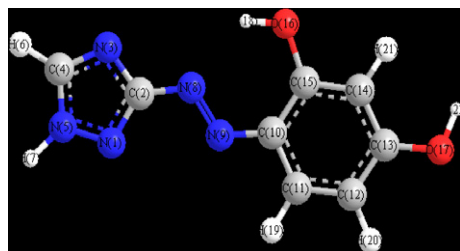
L-ascorbic acid is a well known antioxidant, a reducing agent, a powerful electron donor is known to play a vital role in a number of chemical, biological and physiological reactions in the human body and used as standard antioxidant (positive control). Blank sample was run without ABTS and using instead of tested compounds while negative control was run with ABTS and MeOH/phosphate buffer (1:1) only [53].

Some azo ligands and their copper complexes were subjected to anti-oxidant assay by ABTS method and experimental data were tabulated in Table (S14) and illustrated in Fig. 7. From the data obtained experimentally, we can derive these points:

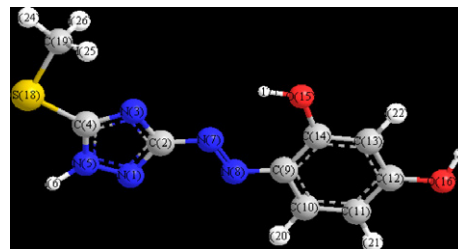
- All complexes subjected to antioxidant assay were less potent active antioxidant agents compared to corresponding azo ligands, the reason may be related to the consumption of free electrons in coordination.
- As increasing number of sulphur atoms in compounds under study, their reactivity increased which was shown from results that HL⁴ was the highest active one than HL² which may be related to the high electronegativity of nitrogen atom than sulphur one.

Conclusion

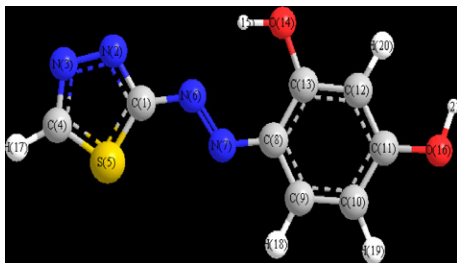
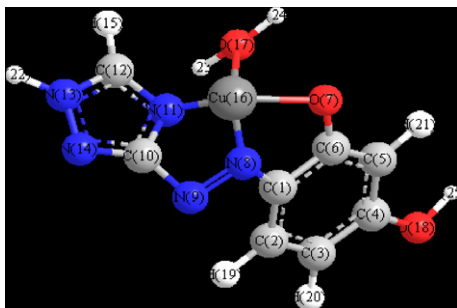
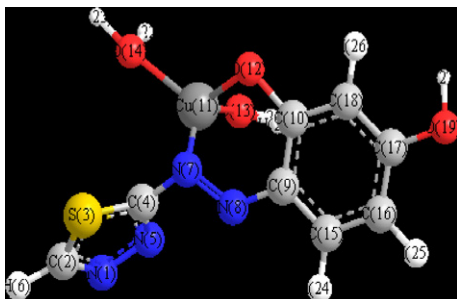
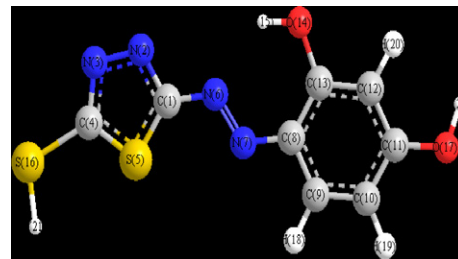
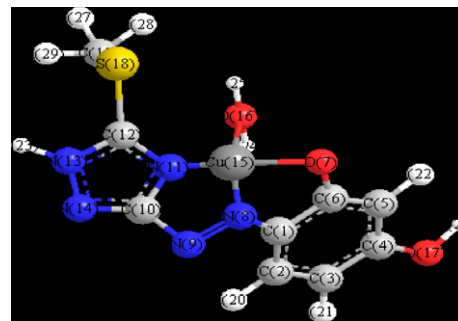
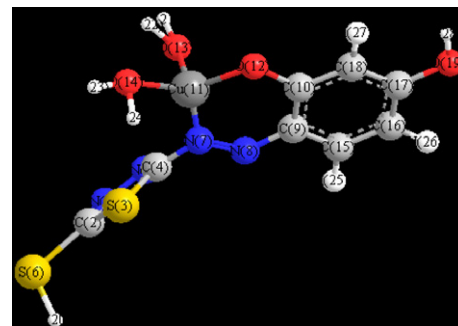
The structure assignment of Cu(II) complexes under investigation was carried out using the elemental analysis, molar conductivity, spectroscopic data (IR, UV–Vis, ESR), magnetic measurements and thermal analysis (TG). The IR spectra showed that the triazole azodyes behave as mono basic tridentate ligands with ONN donor sites while the thiadiazole azodyes behave as mono basic bidentate ligands with ON donor sites. A square planar structure was proposed for Cu(II) complexes C_1 and C_2 and a tetrahedral structure for Cu(II) complexes C_3 and C_4 . The reaction between the azodyes and Cu(II) ion were also studied spectrophotometrically in solution. The stoichiometry and stability constants were evaluated. The analytical data indicated that the investigated azodyes can be used as an indicator for spectrophotometric determination of Cu(II) ion. The calculated bond lengths and bond angles confirmed the structures of Cu(II) complexes. The interaction between the synthesized azo ligands and copper nanoparticles was studied. The spectral data showed the formation of a surface complex between the azodye and colloidal Cu nanoparticles through anchoring –OH[–] group. The antitumor and antioxidant activities of the synthesized azo ligands and their Cu(II) azo complexes have been evaluated.



Structure 1: Molecular model of HL¹



Structure 2: Molecular model of HL²

Structure 3: Molecular model of HL³Structure 5: Molecular model of Cu (II) complex C₁Structure 7: Molecular model of Cu (II) complex C₃Structure 4: Molecular model of HL⁴Structure 6: Molecular model of Cu (II) complex C₂Structure 8: Molecular model of Cu (II) complex C₄

Appendix A. Supplementary material

Supplementary data associated with this article can be found, in the online version, at <http://dx.doi.org/10.1016/j.saa.2013.01.039>.

References

- [1] A.M. khedr, M. Gaber, R.M. Issa, H. Erten, *Dyes Pigments* 67 (2005) 117–126.
- [2] A.M. khedr, M. Gaber, *Spectroscopy Lett.* 38 (2005) 431–445.
- [3] N.M. Rageh, *Spectrochim. Acta A* 60 (2004) 1917–1924.
- [4] M. Tuncel, H. Kahyaoglu, M. Cakir, *Transit. Metal Chem.* 33 (2008) 605–613.
- [5] Y.M. Issa, W.F. El-Hawary, A.F.A. Youssef, A.R. Senosy, *Spectrochim. Acta A* 75 (2010) 1297–1303.
- [6] M.S. Masoud, E.A. Khalil, A.M. Hafez, A.F. El-Husseiny, *Spectrochim. Acta A* 61 (2005) 989–993.
- [7] R. Gup, E. Giziroglu, B. Kirkan, *Dyes Pigments* 73 (2007) 40–46.
- [8] M. Gaber, A.M. Hassanein, A.A. Lotfalla, *J. Mol. Struct.* 875 (2008) 322–328.
- [9] M. Gaber, K. El-Baradie, Y.S. El-Sayed, *Spectrochim. Acta A* 69 (2008) 534–541.
- [10] K. Nejati, Z. Rezvani, M. Seyedahmadian, *Dyes Pigments* 83 (2009) 304–311.
- [11] M.S. Masoud, A. El-Merghany, A.M. Ramadan, M. Abd El-Kaway, *J. Therm. Anal. Calorim.* 101 (2010) 839–847.
- [12] M.S. Sujamol, C.J. Athira, Y. Sindhu, K. Mohanan, *Spectrochim. Acta A* 75 (2010) 106–112.
- [13] M. Gaber, G.B. El-Hefnawy, M.A. El-Borai, N.F. Mohamed, *J. Therm. Anal. Calorim.* 109 (2012) 1397–1405.
- [14] S. Ferrer, R. Ballesteros, A. Sanbartolome, M. Ggonzales, G. Alzuet, *J. Inorg. Biochem.* 98 (2004) 1436–1446.
- [15] F. Gaccioli, R.F. Gazzola, M. Lanfranchi, L. Marchio, G. Metta, M.A. Pellinghelli, S. Tardito, M. Tegoni, *J. Inorg. Biochem.* 99 (2005) 1573–1584.
- [16] A. Demirbas, D. Sahin, N. Demirbas, S. Karaoglu, *Eur. J. Med. Chem.* 44 (2009) 2896–2903.
- [17] Z. Chohan, S. Sumrra, M. Toussoufi, T. Hadda, *Eur. J. Med. Chem.* 45 (2010) 2739–2747.
- [18] A.M. Khedr, M. Gaber, E.H. Abd El-ZaherChin, *J. Chem.* 29 (2011) 2421–2427.
- [19] A. Singh, O. Pandey, S. Sengupta, *Spectrochim. Acta A* 85 (2012) 1–6.
- [20] H. Guo-Qiang, H. Li, X. Song-Qiang, H. Wen-Long, *Chin. J. Chem.* 26 (2008) 1145–1149.
- [21] B.S. Holla, B. Veerendra, M.K. Shivanada, B. Poojary, *Eur. J. Med. Chem.* 38 (2003) 759–767.
- [22] A. Mavrova, D. Wesselinova, Y. Tsenov, P. Denkova, *Eur. J. Med. Chem.* 44 (2009) 63–69.
- [23] M. Noolvi, H. Patel, N. Singh, A. Gadad, S. Cameotra, A. Badiger, *Eur. J. Med. Chem.* 46 (2011) 4411–4418.
- [24] R.H. Lee, E. Griswold, J. Kleinberg, *Inorg. Chem.* 3 (1964) 1278–1283; M.S. Masoud, E.A. Khalil, A.M. Hindawy, A.E. Ali, E.F. Mohamed, *Spectrochim. Acta A* 60 (2004) 2807–2817.
- [25] A. Athawale, P. Katre, M. Kumar, M. Majumdar, *Mater. Chem. Phys.* 91 (2005) 507–512.
- [26] Hyperchem version 8.0 Hypercube, Inc.
- [27] P. Suppan, *J. Chem. Soc. A* (1968) 3125–3133.
- [28] H. Kocaokutgen, S. Ozkinali, *Dyes Pigments* 63 (2004) 83–88.
- [29] M. Sujamol, C. Athira, Y. Sindhu, K. Mohanan, *Spectrochim. Acta A* 75 (2010) 106–112.
- [30] J.H. Yoe, A.L. Jones, *Ind. Eng. Chem. Analyst. Edit.* 16 (1944) 111–115.
- [31] G.H. Ayers, B.D. Narang, *Anal. Chim. Acta* 24 (1961) 241–249.
- [32] A. Harvey, D. Manning, *J. Am. Chem. Soc.* 72 (1950) 4488–4493.
- [33] A.Z. Ringbom, *Z. Anal. Chem.* 115 (1939) 332–343.
- [34] H. Benesi, J. Hildbrand, *J. Am. Chem. Soc.* 71 (1949) 2703–2707.
- [35] A. Kathiravan, R. Renganathan, S. Anandan, *Polyhedron* 28 (2009) 157–161.
- [36] A. Kathiravan, R. Renganathan, *J. Colloid Interf. Sci* 331 (2009) 401–407.

- [37] M. Jhonsi, A. Kathiravan, R. Renganathan, J. Mol. Struct. 921 (2009) 279–284.
- [38] W.J. Geary, Coord. Chem. Rev. 7 (1971) 81–122.
- [39] A.B.P. Lever, Inorganic Electronic Spectroscopy, second ed., Elsevier Science, Amsterdam, 1984;
- A.A. El-Asmy, G.A. Al-Hazmi, Spectrochim. Acta A 71 (2009) 885–1890.
- [40] B.J. Hathaway, D.E. Billing, Coord. Chem. Rev. 5 (1970) 143–207.
- [41] A.D. Kivelson, R. Neiman, J. Chem. Phys. 35 (1961) 149–155.
- [42] B.J. Hathaway, Struct. Bond. 14 (1973) 49–67.
- [43] N.T. Madhu, P.K. Radhakrishnan, E. Williams, W. Linert, J. Therm. Anal. Calorim. 79 (2005) 157–161.
- [44] A.W. Coats, J.P. Redfern, Nature 201 (1964) 68–69.
- [45] H.H. Horowitz, G. Metzgar, Anal. Chem. 35 (1963) 1464–1468.
- [46] W.S. Lopes, C.R. Morais, A.G. de Souza, V.D. Leite, J. Therm. Anal. Calorim. 79 (2005) 343–347.
- [47] V. Satava, Thermochim. Acta 2 (1971) 423–428.
- [48] M.S. Refat, I.M. El-Deen, I. Grabchev, Z.M. Anwer, S. El-Ghol, Spectrochim. Acta A 72 (2009) 772–782.
- [49] S. Ahmed, O. El-Gammal, G. Abu El-Reash, Spectrochim. Acta A 83 (2011) 17–27.
- [50] R.H. Abu-Eittah, N.G. Zaki, M.A. Mohamed, L.T. Kamel, J. Anal. Appl. Pyrol. 77 (2006) 1–11.
- [51] S. Sagdinc, B. Koksoy, F. Kandemirli, S. Bayari, J. Mol. Struct. 917 (2009) 63–70.
- [52] A. Despaigne, J.Da. Sliva, A. Do-Carmo, O. Piro, E. Castllano, H. Beraldo, J. Mol. Struct. 920 (2009) 97–102.
- [53] B.F. Abdel-Wahab, G.A. Awad, F.A. Badria, Eur. J. Med. Chem. 46 (2011) 1505–1511.